The impact of binary water-CO2 isotherm models on the optimal performance of sorbent-based direct air capture processes.

John Young[a], Enrique García-Díez[a], Susana Garcia[a], Mijndert van der Spek[a]

[a]Research Centre for Carbon Solutions, Heriot-Watt University, Edinburgh, EH14 4AS, United Kingdom

ABSTRACT

Direct air capture (DAC) is an auspicious technology in pursuing negative CO_2 emissions. A promising process is temperature vacuum swing adsorption (TVSA) employing amine functionalised adsorbents such as Lewatit® VP OC 1065, which is selected as a benchmark sorbent in this study. To further improve process design, and critically lower costs, detailed modelling of DAC cycles is imperative. However, the multi-component adsorption on these materials, particularly the cooperative adsorption of CO_2 and H_2O, is crudely understood, and yet to be described in mathematical terms, prohibiting sound modelling efforts. Here, we commit in-depth understanding of the effect of humidity on CO_2 adsorption and demonstrate how this impacts modelling of DAC cycles. We present two novel mechanistic co-adsorption isotherm models to describe water's effect on CO_2 adsorption and find a good fit to original experimental co-adsorption data. We also show the considerable improvement in predictions of these models when compared to an empirical co-adsorption isotherm model from literature. A detailed TVSA DAC cycle process model is then used elucidating how different co-adsorption models affect the predicted process performance. It is found that the two novel isotherm models generate similar results and Pareto fronts, whilst the minimum work equivalent calculated using the more conservative of the two models is found to be 2.49 MJ kg^{-1} for the case study considered. These mathematical descriptions laid out will lead to more accurate modelling and optimisation of cyclic DAC adsorption processes, prompting a greater understanding of the material-process combinations ideal for DAC and how costs can be driven down in the years to come. Importantly, they allowed us to independently benchmark a Climeworks type DAC process, providing key DAC performance data to the public domain.

Email: jpy1@hw.ac.uk   RCCS, Heriot-Watt University

1   INTRODUCTION

Anthropogenic greenhouse gas (GHG) emissions are causing the dramatically rising temperature of our planet. The level of atmospheric CO_2 and other GHGs has become untenable, and drastic action is required to prevent a global temperature rise of 1.5 °C, which has been identified as an important limit by the Intergovernmental Panel on Climate Change (IPCC).[1] Negative emissions technologies (NETs) that actively remove CO_2 from the atmosphere will be needed to mitigate hard-to-abate and historical emissions and to reach the Paris Agreement targets.[2,3] Carbon capture and storage (CCS) has a significant role to play in the development and deployment of NETs. Two promising NETs rely on CCS technology. These are bioenergy with carbon capture and storage (BECCS) and direct air capture (DAC).[4] DAC aims to capture CO_2 directly from ambient air resulting in net negative emissions if the CO_2 is permanently stored.[5] Realmonte et al. explored the role DAC can play in a 1.5 °C scenario and emphasise the economic benefit that DAC provides.[5] The study finds that policymakers require much lower carbon prices when DAC is available as a technology. However, the authors of this study stress that DAC should be developed alongside other solutions since significant technical challenges exist.

1.1   CHALLENGES IN SORBENT-BASED DAC PROCESS DESIGN

Here, we focus on direct air capture of CO_2 using amine functionalised adsorbents in temperature vacuum swing adsorption (TVSA) processes. Thus far, much research effort in this space has gone to the development of effective, robust and cheap sorbent materials. More information is available in the supplementary information, as well as Table S1 which summarises some of the materials studied for DAC to date. Beyond sorbent development, the main current challenge for adsorbent-based DAC technologies is to further optimise their process design to enhance efficiency and reduce cost. For this, two critical elements are needed: i) detailed cyclic adsorption process modelling to find optimal process cycles and operating parameters, requiring ii) accurate mathematical descriptions of the underlying adsorption of each adsorbed component, with a focus on the interaction between CO_2 and H_2O. Without accurate adsorption descriptions, there is simply little point in undertaking process design studies.

The two facets governing adsorption that need to be mathematically described are adsorption equilibrium and dynamics (i.e., mass transfer), and this is done using isotherm and kinetic models, respectively. Casas et al. explain that adsorption process modelling is susceptible to small errors in isotherm models, emphasising the importance of an accurate description, and developing the required isotherm models will be one of the objectives of this work.[6] As humidity in air is reported to enhance the equilibrium adsorption of CO_2 on amine-functionalised adsorbents, it is pivotal to describe this interaction correctly.[7–10] However, a mechanistically consistent mathematical description of this enhancement does not yet exist, impeding accurate modelling of DAC processes, and therefore their further improvement.

Email: jpy1@hw.ac.uk   RCCS, Heriot-Watt University

62   Here, we aim to fill the caveats in understanding and modelling of water-CO_2 interactions, by
63 deriving mechanistically consistent co-adsorption models, showing how the use of different models
64 influences the modelling of DAC adsorption cycles and thus their technical performance. To this end,
65 we combined adsorption theory with new experiments and modelling studies. The paper is structured
66 as follows: first, the theoretical mechanisms and their implications for CO_2 adsorption onto amine-
67 functionalised sorbents are discussed to allow the derivation of sound (co-)adsorption isotherm models.
68 Second, accurate representations of pure component and co-adsorption isotherms were measured
69 experimentally and fit to the co-adsorption isotherm models. Finally, the isotherm models were used in
70 a detailed process model to demonstrate how the different descriptions affect process performance and
71 assert that sound descriptions of the physical processes are indeed critical to the design of efficient
72 sorbent-based DAC plants.

73   In this work we use Lewatit® VP OC 1065 as an example of a typical primary amine-functionalised
74 adsorbent and we suggest henceforth to use this sorbent as a *benchmark* for DAC purposes. A key
75 reason to select this sorbent is its commercial availability, and therefore accessibility to any interested
76 party, besides being believed to be (very similar to) the adsorbent that Climeworks uses in their first-
77 generation DAC process.*

2   THEORY OF CO_2 AND H_2O ADSORPTION ONTO AMINE-FUNCTIONALISED ADSORBENTS

2.1 PURE COMPONENT ADSORPTION

2.1.1 CO_2 isotherms

82   Adsorption equilibrium of species onto a solid surface is typically described by isotherm models. A
83 standard isotherm model used to describe CO_2 adsorption on amine-functionalised adsorbents is the
84 temperature-dependent Toth isotherm which has previously been used for amine functionalised silica,
85 cellulose, and Lewatit® VP OC 1065.[7,11–13] This is an empirical extension to the Langmuir isotherm,
86 which improves the fit at the lowest and highest pressure ranges,[14] the lowest region being specifically
87 relevant for amine functionalised sorbents due to their high affinity for CO_2. The equations defining the
88 temperature-dependent form of the Toth isotherm are given in Equations 1-4.

---

*Climeworks' patent describing the kind of material that may be used in their process and simultaneously
supplying an accurate description of Lewatit® VP OC 1065: "polystyrene matrix material modified with amine
groups, specifically primary amine groups".[57]

Email: jpy1@hw.ac.uk   RCCS, Heriot-Watt University

$$q_{CO_2} = \frac{q_\infty(T)b(T)p_{CO_2}}{\left(1 + \left(b(T)p_{CO_2}\right)^{\tau(T)}\right)^{\frac{1}{\tau(T)}}}$$

<div align="right">1.</div>

89

90   Where q_{CO_2} [mol kg^{-1}] is the loading of CO_2 on the adsorbent, q_∞ [mol kg^{-1}] is maximum CO_2

91   capacity, b [Pa^{-1}] is the affinity of CO_2 to the adsorbent, p_{CO_2}[Pa] is the partial pressure of CO_2, and τ

92   [-] is an exponential factor to account for surface heterogeneity. The maximum CO_2 capacity of the

93   sorbent is defined by Equation 2.

$$q_\infty(T) = q_{\infty,0} \exp\left(\chi\left(1 - \frac{T}{T_0}\right)\right)$$

<div align="right">2.</div>

94

95   Where $q_{\infty,0}$ [mol kg^{-1}] is q_∞ at the reference temperature T_0 [K], T [K] is the temperature, and χ [-]

96   is a factor used to describe the temperature dependency.

97

98   The affinity of the sorbent to CO_2 is defined by Equation 3.[†]

$$b(T) = b_0 \exp\left(\frac{-\Delta H_0}{RT}\right)$$

<div align="right">3.</div>

99   Where b_0 [Pa^{-1}] is a pre-exponential affinity parameter, ΔH_0 [J mol^{-1}] is the isosteric heat of

100   adsorption, and R [J mol^{-1} K^{-1}] is the universal gas constant. Finally, the surface heterogeneity parameter

101   is defined in Equation 4.

$$\tau(T) = \tau_0 + \alpha\left(1 - \frac{T_0}{T}\right)$$

<div align="right">4.</div>

102

103   Where τ_0 [-] is τ at the reference temperature, and α [-] is a factor used to describe the temperature

104   dependency.

105   2.1.2   H₂O isotherms

106   Adsorption of water onto solid species is an interesting field of study itself and is essential for CO_2

107   capture applications. The work by Hefti et al.,[15–18] provides a very relevant body of knowledge. Water

108   adsorption on Lewatit® VP OC 1065 follows a typical Type III isotherm, with hysteresis loops of Type

109   H3, according to the IUPAC classification.[19] The isotherms can be seen in Figure S10, in the

---

[†] The equation more commonly used to describe this parameter[13] has been re-arranged in this work, which also changes the meaning of b_0. The original equation causes the relationship between ΔH_0 and b to be dependent on the arbitrarily assigned T_0. For this reason, the equation has been changed to remove this dependence, and the motivation becomes apparent in Section 2.3.1, where ΔH_0 is a parameter that varies due to co-adsorption.

110 supplementary information. This behaviour is typical for unrestricted monolayer-multilayer adsorption
111 of the water onto favourable sites of a macroporous adsorbent.

112 We chose an isotherm model that is commonly used to describe this behaviour, i.e., the Guggenheim-
113 Anderson-de Boer (GAB) model.[7,13,20] This model is an extension to the widely utilised Brunauer-
114 Emmett-Teller (BET) equation. [61] The derivation of the BET equation assumes that the first layer of
115 adsorption has a heat of adsorption that is different from every subsequent layer, whilst the subsequent
116 layers have a heat of adsorption equivalent to the latent heat of condensation. Meanwhile, the GAB
117 model improves this by assuming that only the 10th layer onwards has a heat of adsorption equal to the
118 latent heat of condensation, whilst the 2nd to 9th layers have a heat of adsorption that is different to the
119 first layer. Equation 5 presents the GAB isotherm model:

$$q_{H_2O} = \frac{q_m k c x}{(1 - kx)(1 + (c - 1)kx)} \qquad 5.$$

120 Where q_{H_2O} [mol kg^{-1}] is the loading of water, q_m [mol kg^{-1}] is the loading that corresponds to a
121 monolayer, k [-], and c [-] are affinity parameters, and x [-] is the relative humidity.

122 Some studies do not consider temperature dependency beyond its effect on relative humidity with k
123 and c as constant values.[13,15] Other studies describe the temperature dependency of k and c according
124 to Anderson's derivation.[7,16,20,21] These descriptions as they appear in Anderson's derivation are shown
125 in Equations 6-7.[21,22] Note that the pre-exponential factors used in the recent studies by Gebald et al.[7]
126 and Wurzbacher et al.[20] are dropped to present the description according to Anderson's derivation.

$$c = \exp\left(\frac{E_1 - E_{10+}}{RT}\right) \qquad 6.$$

127 Where E_1 [J mol^{-1}] is the heat of adsorption of the first layer of adsorption, and E_{10+} [J mol^{-1}] is the
128 heat of adsorption of the 10th layer and higher, which is equivalent to the latent heat of condensation of
129 water.

$$k = \exp\left(\frac{E_{2-9} - E_{10+}}{RT}\right) \qquad 7.$$

130 Where E_{2-9} [J mol^{-1}] is the heat of adsorption of the 2nd to 9th layer.

131 The picture is further complicated when it is considered that the heats of adsorption of the different
132 layers may also be dependent on temperature, as is found by Anderson and Hall.[22] Indeed, we know
133 that the heat of condensation for water, or E_{10+}, depends on temperature.

134 Here, we chose to incorporate the temperature dependency because our experimental results show a
135 temperature-dependency beyond that taken into account by relative humidity, see Figure S10 in the
136 supplementary information, as was also found earlier by Gebald et al. for amine-functionalised

cellulose.[7] Up to 100 °C, the thermal stability limit of Lewatit® VP OC 1065,[23] we fitted the heat of condensation for water to the correlation shown by Equation 8 using experimental data from NIST.[24]

$$E_{10+} = -44.38T + 57220 \qquad\qquad 8.$$

Consequently, to fit an accurate version of the GAB equation, the unknown dependencies of temperature on E_1 and E_{2-9} were empirically fitted to the experimental water isotherms measured in this study.

2.2   EFFECT OF HUMIDITY ON CO_2 ADSORPTION

On amine-functionalised adsorbents, it has been shown that CO_2 has little impact on H_2O equilibrium adsorption up to relative humidities of at least 60%.[7,8,25] However, previous studies have shown that H_2O enhances CO_2 adsorption significantly.[7–9,26,27]

The underlying chemical mechanisms need to be understood in detail to mathematically explain the co-adsorption of CO_2 and H_2O on amine-functionalised sorbents. Thus far, there has been only one attempt to develop an empirical mathematical description by Stampi-Bombelli et al.,[13] further discussed in 2.3.3. Meanwhile, Jung and Lee derived an isotherm model from kinetics specifically for ammonium carbamate and bicarbonate formation.[28] However, there is no one adsorption mechanism that is valid for all amine-functionalised sorbents, and actually, there may be multiple mechanisms in play on one adsorbent.

Here, we briefly discuss the key mechanisms used to derive mechanistically consistent co-adsorption isotherm models. The mechanisms are threefold: the change of amine efficiency (i.e., CO_2 adsorption stoichiometry); a change in the heat of adsorption, also affecting the sorbent's affinity to CO_2; and amine site blocking by adsorbed water molecules.

2.2.1   Three governing mechanisms

Existing literature has repeatedly reported the two species formed on amine functionalised adsorbents in the presence of carbon dioxide, and these are shown in Figure 1.
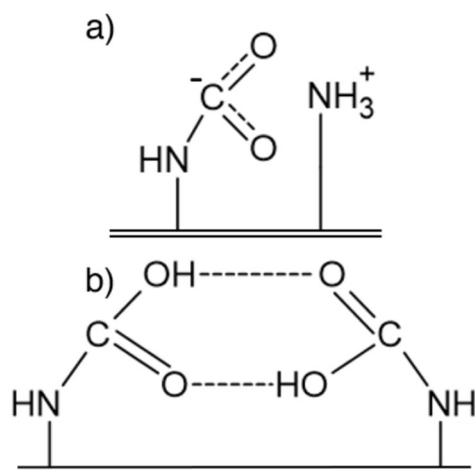
Email: jpy1@hw.ac.uk   RCCS, Heriot-Watt University

Figure 1 Species that CO$_2$ adsorbs as on amine-functionalised sorbents in the absence of water. a) Ammonium carbamate. b) Paired carbamic acid

161

162 Figure 1a) shows an ammonium carbamate ionic pair, which forms from an ammonium carbamate

163 zwitterion precursor requiring two amine groups per adsorbed CO$_2$ molecule.[25,27,29–32] Meanwhile, 1b)

164 is a pair of carbamic acid species stabilising each other via hydrogen bonding.[25,27,31,33,34] The carbamic

165 acid requires stabilisation as it tends to convert back to CO$_2$ and an amine group.[35] Yu and Chuang

166 indicated that carbamic acid formation was primarily associated with secondary amines, using in-situ

167 FT-IR spectroscopy. However, there is not enough evidence to rule out carbamic acid forming on

168 primary amines.[27] Indeed, the molecular modelling study by Buijs and De Flart in 2017 concluded that

169 for the primary-amine based Lewatit® VP OC 1065, the formation of ammonium carbamate is unlikely,

170 with the carbamic acid formation being a more favourable pathway. Although Alesi and Kitchin found,

171 experimentally, that it was inconclusive as to whether carbamic acid or ammonium carbamate formation

172 is the dominant mechanism on Lewatit® VP OC 1065.[36,37] In reality, it may be that many different

173 species form on one amine-functionalised sorbent, which is shown to be possible by Yu and Chuang.[27]

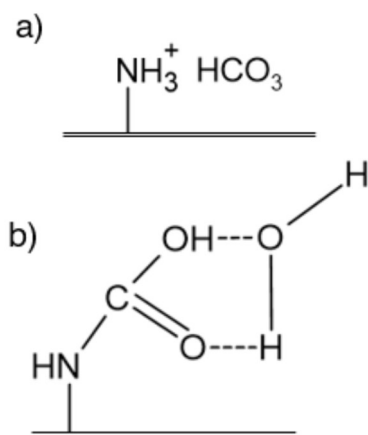Email: jpy1@hw.ac.uk   RCCS, Heriot-Watt University

Figure 2 Additional species that CO₂ adsorbs as on amine-functionalised sorbents in the presence of water. a) Ammonium bicarbonate. b) Water stabilised carbamic acid

174

Figure 2 presents the additional adsorbed species of CO_2 that form in the presence of water. Figure 2a) shows ammonium bicarbonate, which forms from a paired ammonium carbamate precursor.[25,27] Li et al. suggest that, instead of ammonium bicarbonate formation, hydronium carbamate could also be formed from ammonium carbamate.[38] The effect on adsorption is very similar for both these pathways, as each species only requires one amine group for CO_2 adsorption, as opposed to two for ammonium carbamate. Finally, 2b) shows a carbamic acid that is stabilised by a water molecule rather than another carbamic acid.[27]

Kinetics may also play a role in the speciation of adsorbed carbon dioxide on amine-functionalised adsorbents. Didas et al. observed that the formation of ammonium bicarbonate is much slower than the formation of ammonium carbamate.[25] However, to the best of our knowledge, this has yet to be confirmed for hydronium carbamate. If ammonium bicarbonate does form more slowly from an ammonium carbamate precursor, we would expect an initially fast uptake of CO_2 until the amount of ammonium carbamate reaches equilibrium, before the uptake slowly increases further as the ammonium carbamate is converted to ammonium bicarbonate. Aside from chemical kinetics, the presence of water may also inhibit or enhance the diffusion of CO_2 to the amine sites affecting the overall kinetics of the adsorption process. This requires further investigation but is beyond the scope of this study.

For independent water adsorption, water molecules hydrogen bond onto the amine groups as the first adsorption layer with multiple layers forming on top also via hydrogen bonding as shown in Figure 3.[27]
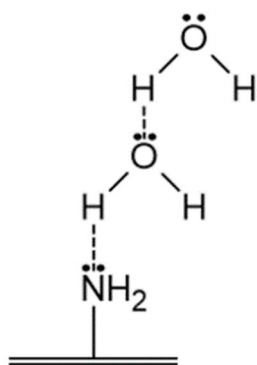
193

Email: jpy1@hw.ac.uk   RCCS, Heriot-Watt University

Figure 3 Hydrogen bonding of water onto supported amine groups

194

195   The above-explained chemistry determines a key concept in CO_2 adsorption onto amine sorbents,

196 namely amine efficiency. Amine efficiency has previously been defined as the number of CO_2

197 molecules adsorbed divided by the total number of amine groups available.[25,30,39–42] For the formation

198 of ammonium carbamate pairs, the theoretical maximum amine efficiency is 0.5 since this is the

199 stoichiometric ratio of CO_2 adsorbed to amine groups required. However, when ammonium bicarbonate

200 or hydronium carbamate forms, the theoretical maximum amine efficiency or stoichiometric ratio

201 increases to 1. For this reason, the amine efficiency can be enhanced in the presence of water.

202   Besides amine efficiency, humidity has also shown to affect the heat of adsorption of adsorbed

203 species. Yu and Chuang utilised temperature-programmed desorption to calculate each species' binding

204 energy, which is equivalent to the heat of desorption. The calculations find that the binding energy

205 increases in this order: water stabilised carbamic acid < adsorbed water < paired carbamic acid ≈

206 ammonium carbamate pair.[27] Their results show an apparent decrease in the overall heat of desorption

207 in the presence of water occurring through a reduction in the binding energy of ammonium carbamate,

208 and a promotion in the formation of ammonium bicarbonate. However, they also suggest that the

209 presence of water increases the binding of paired carbamic acid and promotes its formation over other

210 species leading to an overall increase in the heat of adsorption.

211   The heat of adsorption is not only relevant as a standalone quantity, but it also influences the uptake

212 equilibrium, particularly the affinity constant of isotherms (see Section 2.1.1). For example, in the

213 modified temperature-dependent version of the Toth model, shown in Equations 1-4, an increase in the

214 magnitude of the heat of adsorption leads a larger affinity constant of the isotherms and vice versa.[12]

215 The affinity constant is a measure of the gradient of the isotherm at low partial pressures. As a result,

216 an increase in the heat of adsorption would lead to higher uptakes under DAC conditions because of the

217 very low CO_2 concentrations in air.

218   Finally, we hypothesise there may be a third effect at play. This is water multilayers blocking CO_2

219 access to amine sites, which could affect kinetics and equilibrium uptake alike. Didas et al. observed

Email: jpy1@hw.ac.uk   RCCS, Heriot-Watt University

that water can have a negative impact on CO_2 uptake at low partial pressures of CO_2 for the amine-functionalised silica they studied with the highest amine coverage.[25] We propose that the high amine coverage led to the agglomeration of water multilayers, formed on the amines, preventing CO_2 from accessing the amine sites.

2.3 WATER-CO_2 CO-ADSORPTION MODELS

The complexities in determining the exact species formed on adsorption, prevent us from using the classical kinetic approach to deriving an isotherm model. Hence, based on the above discussion, we propose two different models to consistently describe water-CO_2 co-adsorption, which we call the mechanistic co-adsorption model and the weighted average dual site Toth (WADST) model. We also discuss a recently published empirical co-adsorption model by Stampi-Bombelli et al.[13] Here onwards, we assume that water affects CO_2 adsorption, but CO_2 does not affect water adsorption. There is previous experimental evidence to support this assumption.[7,8,43]

2.3.1 Mechanistic co-adsorption model

To summarise, the main three effects discussed so far are:

1. At high water loadings, amine efficiency may be limited by hydrogen-bonded water structures blocking CO_2 access to amine sites.
2. The presence of water can increase the stoichiometric ratio due to ammonium bicarbonate forming rather than ammonium carbamate.
3. The presence of water changes the heats of adsorption of adsorbed CO_2 species hence the affinity.

Based on these three effects, we propose the mechanistic adjustment of isotherm behaviour described in Equations 9-13. First, we postulate a generic equation of CO_2 loading including terms for the amine efficiency under actual, ϕ [-], and dry, ϕ_{dry} [-] conditions:

$$q_{CO_2} = \frac{\phi}{\phi_{dry}} f(p_{CO_2}, T, \Delta H_{ave}) \tag{9.}$$

Where f is the temperature and partial pressure-dependent isotherm equation, and ΔH_{ave} [J mol^{-1}] is the average heat of adsorption calculated in Equation 13.

Secondly, effect 1 can be described as the fraction of the sites blocked by hydrogen-bonded water structures deducted from the theoretical maximum available sites, i.e., under zero site blockage, to calculate the fraction of amine sites available for adsorption as in Equation 10.

$$\phi_{available} = \phi_{max} - f_{blocked} \tag{10.}$$

Email: jpy1@hw.ac.uk   RCCS, Heriot-Watt University

249   Where $\phi_{available}$ [-] is the fraction of sites available for adsorption, and ϕ_{max} [-] is the maximum

250   possible amine efficiency, which can be assumed to be 1 (recall this is the maximum theoretical

251   efficiency). The fraction of the sites blocked, $f_{blocked}$ [-] must now be calculated.

252   Thirdly, the fraction of amine sites blocked should be proportional to the size of adsorbed water

253   aggregates. The size of these aggregates adsorbed is further related to the loading of water on the

254   adsorbent. We hypothesise that a parallel can be drawn between these aggregates' growth with increased

255   loading and how crystals grow with time. Crystals nucleate and grow slowly at first. Then when the

256   particles are of sufficient size, they begin to aggregate, speeding up the growth. At small loadings,

257   increasing loading may only slightly increase these structures' size before reaching the critical size

258   needed to start forming aggregates. We propose to use Avrami's equation for this purpose, as shown in

259   Equation 11.[44–48]

$$f_{blocked} = f_{blocked,max} \left(1 - e^{-(k q_{H_2O})^n}\right) \qquad 11.$$

260   Where $f_{blocked,max}$ [-], k [kg mol^{-1}], and n [-] are parameters to be fitted.

261   Next, is to describe the increase in the stoichiometric ratio and amine efficiency. As the loading of

262   water increases, the fraction of the sites that exist with a convenient water molecule for stabilised

263   carbamic acid or ammonium bicarbonate formation increases. We suggest that a Maxwell-Boltzmann

264   distribution could describe this.[49,50] This distribution is used for many things relating to the probability

265   of two states, including economics.[51] Another example is chemical kinetics, where it is used to show

266   how, with an increase in temperature, a higher proportion of molecular collisions have the required

267   energy for a reaction to occur (the well-known Arrhenius' law). Henceforth, we suggest applying the

268   Maxwell-Boltzmann distribution to our case providing Equation 12.

$$\phi = \phi_{dry} + \left(\phi_{available} - \phi_{dry}\right)e^{-\frac{A}{q_{H_2O}}} \qquad 12.$$

269   Here A [mol kg^{-1}] is a critical water loading value that must be fitted as well as ϕ_{dry} [-].

270   Finally, the heat of adsorption can be calculated by taking a weighted average between the wet and

271   dry states. Since $e^{-\frac{A}{q_{H_2O}}}$ is equal to the fraction of sites that form adsorbed species with water, the

272   weighted average appears as in Equation 13.

$$\Delta H_{ave} = \left(1 - e^{-\frac{A}{q_{H_2O}}}\right)\Delta H_{dry} + e^{-\frac{A}{q_{H_2O}}}\Delta H_{wet} \qquad 13.$$

273   Where ΔH_{dry} [J mol^{-1}] and ΔH_{wet} [J mol^{-1}] are the heats of adsorption in dry and wet states,

274   respectively. ΔH_{dry} can be calculated from pure CO_2 isotherms whilst ΔH_{wet} can be fit to co-

275   adsorption data.

Email: jpy1@hw.ac.uk   RCCS, Heriot-Watt University

2.3.2 Weighted-average dual-site Toth (WADST) co-adsorption model

The derivation of the mechanistic model assumes we know everything about chemisorption of CO_2 and H_2O on amine-functionalised adsorbents, as we stated earlier, this may not yet be the case. Therefore, we propose another approach to modelling CO_2 and H_2O co-adsorption equilibrium that does not depend on these assumptions to create a more general, empirical model. To do this, we shall take a more classical approach to describe co-adsorption. This approach assumes that there are two types of site. One with an available water molecule and one without an available water molecule. Furthermore, the same approach as with the mechanistic model will be used to describe the probability that a site has an available water molecule via an Arrhenius style equation described by the same critical water loading parameter A. This rationale results in Equation 14.

$$q_{CO_2} = \left(1 - e^{-\frac{A}{q_{H_2O}}}\right) \frac{q_{\infty,dry}(T) b_{dry}(T) p_{CO_2}}{\left(1 + \left(b_{dry}(T) p_{CO_2}\right)^{\tau_{dry}(T)}\right)^{\frac{1}{\tau_{dry}(T)}}} + e^{-\frac{A}{q_{H_2O}}} \frac{q_{\infty,wet}(T) b_{wet}(T) p_{CO_2}}{\left(1 + \left(b_{wet}(T) p_{CO_2}\right)^{\tau_{wet}(T)}\right)^{\frac{1}{\tau_{wet}(T)}}} \qquad 14.$$

Here the *dry* site in the isotherm is simply defined by the Toth model shown in Equations 1-4. Meanwhile, the *wet* site is again defined by the same equations and fit, alongside A, to co-adsorption experiments, with the *dry* site already fixed from pure-component isotherms.

2.3.3 Previous empirical co-adsorption model

Stampi-Bombelli et al. presented a useful first endeavour to describe co-adsorption on an amine-functionalised cellulose material by suggesting an empirical adjustment to the pure Toth model.[13] A summary of the adjustment is shown in Equations 15-16.

$$q_\infty\left(T, q_{H_2O}\right) = q_\infty(T) \left(\frac{1}{1 - \gamma q_{H_2O}}\right) \qquad 15.$$

$$b\left(T, q_{H_2O}\right) = b(T)\left(1 + \beta q_{H_2O}\right) \qquad 16.$$

Here γ [-] and β [-] do not have any specific physical meaning but are simply the parameters that describe co-adsorption and should be fit to wet experiments. The authors of this study also suggest that γ and β should be greater than 0. However, we suggest that γ could have a negative value to take into account the overall CO_2 capacity reducing due site blockage. This model is virtually the only co-adsorption model that has been investigated before and we include it in our investigations as a comparison for our models in terms of accuracy of describing the co-adsorption phenomenon and cyclic process performance.

3 EXPERIMENTAL METHODS

After formulating the mathematical adsorption equilibrium models, these needed to be parametrised with experimental data, which acquisition is described here.

The material investigated, Lewatit® VP OC 1065, was obtained from Sigma-Aldrich. It is a divinylbenzene (DVB) crosslinked polymer functionalised with primary amine groups. It has an average pore diameter of 25 nm, a bead size of 0.315 – 1.25 mm, pore volume of 0.27 cm^3 g^{-1}, and a surface area of 50 m^2 g^{-1}.[23] Meanwhile, the heat capacity is reported as 1.58 kJ kg^{-1} K^{-1}.[52]
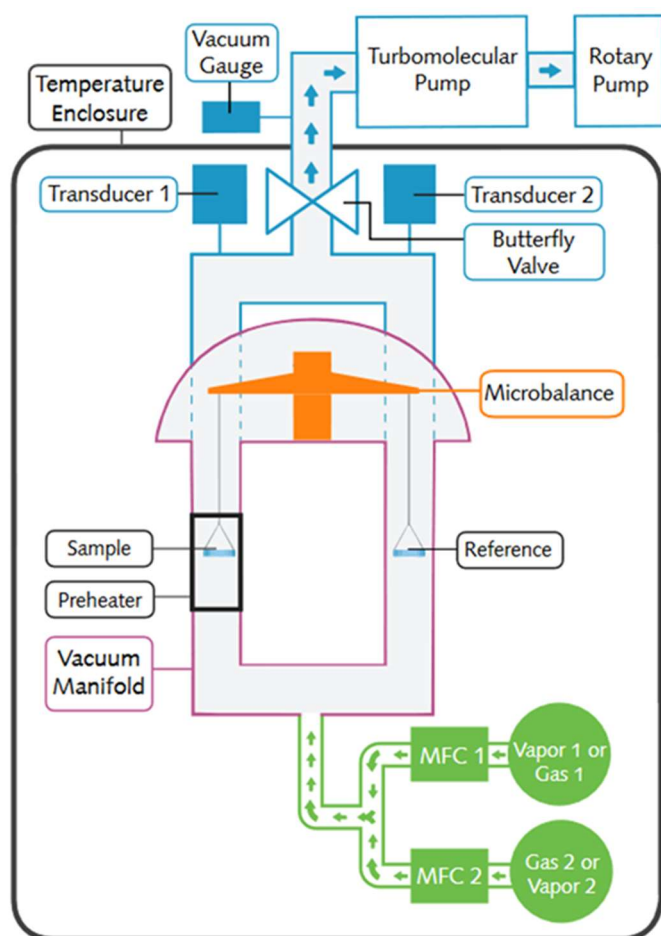

Figure 4 A simple schematic showing the DVS Vacuum. Used with permission of Surface Measurement Systems.[53]

CO_2 and H_2O pure component isotherms and co-adsorption isotherms were measured using the DVS Vacuum system, of which a simple schematic is depicted in Figure 4.[54] The DVS uses a gravimetric, magnetic suspension balance to accurately measure any weight changes as a result of adsorption and desorption. It can operate in dynamic mode with gas flowing through the sorption chamber or static

Email: jpy1@hw.ac.uk   RCCS, Heriot-Watt University

mode where gas is pulsed into the chamber. The DVS utilises a turbomolecular pump which ensures extremely thorough outgassing.

The methodology for measuring pure component isotherms first involved an outgassing step where around 50 mg of sample was heated to 100°C at a pressure of around 1-2 Pa for at least 10 hours. The sample was then cooled to the desired adsorption temperature before the gas and/or vapour was fed to the device by opening the mass flow controllers. The pressure was increased stepwise up to 1 bar allowing the mass of the sample to equilibrate at each step. CO_2 sorption was studied under semi-static mode, whilst the dynamic mode was used for H_2O sorption. Once 1 bar was reached, the procedure was repeated backwards, i.e., in desorption mode, providing potential hysteresis measurements. A fresh sample of adsorbent was used for every isotherm.

CO_2-water co-adsorption isotherm experiments were undertaken using the DVS Vacuum under the explicit assumption that CO_2 does not affect H_2O equilibrium adsorption. This was demonstrated by Veneman et al. for Lewatit up to a relative humidity of 60%.[8] In addition, there is evidence that this assumption also holds for other types of amine-functionalised adsorbents, such as silica and cellulose.[7,25] For the co-adsorption experiments, the outgassing step was the same, and semi-static mode was used. Then, the sample was first equilibrated with H_2O vapour (for both the 30% and 55% RH experiments). Since CO_2 does not affect H_2O adsorption, the H_2O loading and partial pressure will remain constant for the rest of the experiment, given that no more H_2O is added to the chamber. Hence, further pressure increments were implemented using only CO_2, and semi-static mode was used (i.e., no outlet from the chamber). An example dynamic profile of the experiments is shown in the supplementary information, Figure S2.

Tests were also conducted to check whether the assumption applied here would hold up to 80% relative humidity. However, a sharp initial drop in the mass was observed in the dynamic profile of the experiment when CO_2 was added to the chamber, suggesting the desorption of H_2O. We were unable to determine whether the subsequent adsorption was due to CO_2, H_2O, or both. Further experimental work is currently undertaken to study this phenomenon. An example of this profile is shown in Figure S4. More information about the methodology is available in the supplementary information.

4 DAC PROCESS MODELLING

4.1 PROCESS DESIGN

Using the calibrated adsorption isotherms, we moved to cycle modelling to understand the impact of co-adsorption descriptions on process performance and to provide an independent benchmark of a TVSA DAC cycle. The cycle modelled is shown in Figure 5, where the process is a packed-bed TVSA

Email: jpy1@hw.ac.uk   RCCS, Heriot-Watt University

cycle. The steps of the cycle are as follows: vacuum, heating, a second heating step where the product is extracted (desorption), cooling, pressurisation, and adsorption. The cooling step is important to bring the sorbent temperature to below 90°C before being exposed to air to avoid unnecessary sorbent degradation.[52,55,56] This process is similar to the one, without a steam-purge, used by Stampi-Bombelli et al. with an extra addition of the short cooling step to prolong the sorbent's lifetime.[13] The process is modelled as a very thin, flat packed bed with length L = 1 cm and diameter D = 10 cm. Although a traditional (column type) packed bed is unlikely to be deployed in a real DAC process, the modelling of a flat packed bed can be a realistic approximation to modelling one of the adsorbent plates described in patents from Climeworks.[57]
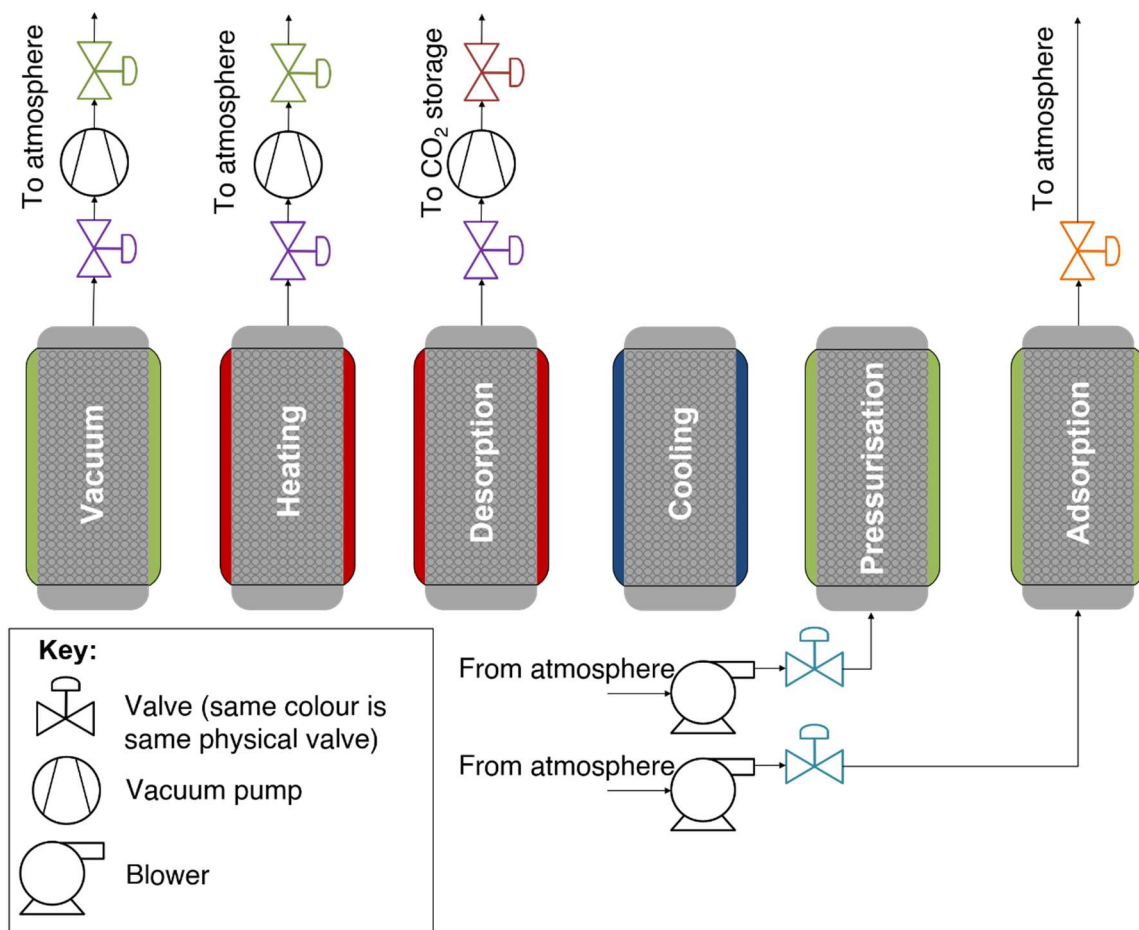

Figure 5 A schematic of the simple DAC TVSA cycle modelled in the case studies. The valves are highlighted in different colours to represent which valves are the same physical valves.

4.2 MODEL ASSUMPTIONS, MASS AND ENERGY BALANCES

A physical model is required to study the dynamics of adsorption within a packed bed. This will allow the fitting of mass transfer coefficients to experimental data and the study of DAC process performance. The model used in this study closely follows the work by Casas et al.[6] Validation work

Email: jpy1@hw.ac.uk   RCCS, Heriot-Watt University

359   can be found in the supplementary information, Figure S18, where the model results are compared to

360   an earlier temperature swing adsorption study from Joss et al.[58]

361   The key assumptions for the model are as follows:

362   • The fluid is an ideal gas.

363   • The flow is described by an axially dispersed plug flow model.

364   • Radial gradients are neglected.

365   • There is instantaneous thermal equilibrium between the fluid and solid pellets.

366   • Mass transfer is described by the linear driving force (LDF) model.[59] The LDF constants are fitted

367   to dynamic data, shown in Figures S16 and S17 of the supplementary information.

368   • Mass transfer coefficients, axial dispersion coefficients, solid heat capacities, and heats of

369   adsorption are independent of temperature.

370   • No N_2 is adsorbed,[‡] and the non-CO2/H2O component of air acts as N_2.

371   • Pressure drop is described by the Ergun equation.[60]

372   The overall mass balance is:

$$\frac{\partial}{\partial z}(vc) + \epsilon_t \frac{\partial c}{\partial t} + (1 - \epsilon_b)\rho_p \Sigma_i \frac{\partial q_i}{\partial t} = 0 \qquad 17.$$

373   Where z [m] is the length along the column, v [m s^{-1}] is the superficial velocity of the fluid, c [mol

374   m^{-3}] is concentration, ϵ_t [-] is the total void fraction in the column, t [s] is time, ϵ_b [-] is the void

375   fraction of the bed, ρ_p [kg m^{-3}] is the density of the pellet, and q_i [mol kg^{-1}] is the loading of

376   component i. The component mass balances are:

$$-D_L \epsilon_b \frac{\partial^2 c_i}{\partial z^2} + \frac{\partial}{\partial z}(vc_i) + \epsilon_t \frac{\partial c_i}{\partial t} + (1 - \epsilon_b)\rho_p \frac{\partial q_i}{\partial t} = 0 \qquad 18.$$

377   Here D_L [m^2 s^{-1}] is the axial dispersion coefficient, and c_i [mol m^{-3}] is the concentration of

378   component i.

379   Next, the energy balance is:

$$-\lambda_L \epsilon_b \frac{\partial^2 T}{\partial z^2} + vc C_{p,f} \frac{\partial T}{\partial z} + \left(\epsilon_t c C_{p,f} + (1 - \epsilon_b)\rho_p\left(C_{p,s} + C_{p,f}\Sigma_i q_i\right)\right)\frac{\partial T}{\partial t} - \epsilon_t \frac{\partial P}{\partial t} \qquad 19.$$
$$= (1 - \epsilon_b)\rho_p \Sigma_i \left((-\Delta H_i)\frac{\partial q_i}{\partial t}\right) - \frac{4h_j}{d}(T - T_j)$$

---

‡ It is experimentally confirmed that the amount of N_2 adsorbed is very low under ambient conditions
(~0.01 mmol g^{-1}). Three isotherms are showing this are found in the supplementary information,
Figure S5. Henceforth, we assume no N_2 is adsorbed.

Email: jpy1@hw.ac.uk   RCCS, Heriot-Watt University

380   Where λ_L [W m^{-1} K^{-1}] is the axial thermal dispersion coefficient, T [K] is temperature, $C_{p,f}$ [J mol^{-1}

381   K^{-1}] is the molar fluid heat capacity, $C_{p,s}$ [J kg^{-1} K^{-1}] is the mass-based adsorbent heat capacity, P

382   [Pa] is pressure, ΔH_i [J mol^{-1}] is the heat of adsorption for component i, h_j [W m^{-2} K^{-1}] is the global

383   heat transfer coefficient between the jacket and the column, d [m] is the diameter of the column, and

384   T_j [K] is the temperature of the jacket.

385   A wall energy balance, like the one presented by Casas et al., is not included in this model.[6]

386   Instead, a global heat transfer coefficient is used to predict the heat transfer from the jacket to the

387   inside of the column. We found that this did not significantly affect the model results during

388   validation and substantially improved the computational speed and robustness. However, it does

389   prevent us from calculating the parasitic sensible heat of the contactor. We would like to stress here

390   that the process presented is a hypothetical one to show the effect of co-adsorption, and further

391   detailed design of the contactor would be required to calculate the sensible heat of the contactor

392   accurately.

393   Other constitutive equations, along with boundary and initial conditions, can be found in the

394   supplementary information.

395   The model calculates the following performance indicators that are relevant to this work:

$$\Phi = \frac{N_{CO_2}}{N_{CO_2} + N_{N_2}} \qquad 20.$$

396

$$Pr = \frac{N_{CO_2}}{V_{bed} t_{cycle}} \qquad 21.$$

397

$$Q_{th} = \frac{\int_{t_{heat,start}}^{t_{des,end}} \frac{\pi D_b^2}{4} \int_0^L \frac{4 h_L}{D_b} (T_w - T) dz\, dt}{N_{CO_2}} \qquad 22.$$

$$W = \frac{\int_{t_{vac,start}}^{t_{vac,end}} \sum_{i=1}^{N_c} n_i(z=L) \frac{1}{\eta_{vac}} \frac{\gamma_{gas}}{1-\gamma_{gas}} RT(z=L) \left(\frac{P_{ambient}}{P(z=L)}^{\frac{\gamma_{gas}-1}{\gamma_{gas}}} - 1 \right) dt}{N_{CO_2}} \qquad 23.$$

$$+ \frac{\int_{t_{vac,start}}^{t_{vac,end}} \sum_{i=1}^{N_c} n_i(z=0) \frac{1}{\eta_{blower}} \frac{\gamma_{gas}}{1-\gamma_{gas}} RT(z=0) \left(\frac{P(z=0)}{P_{ambient}}^{\frac{\gamma_{gas}-1}{\gamma_{gas}}} - 1 \right) dt}{N_{CO_2}}$$

398   Where Φ [-] is purity, N_i [mol] is the total number of moles extracted, as a product, of component i

399   in one cycle, Pr [mol m^{-3} s^{-1}] is productivity, V_{bed} [m^3] is the volume of the bed, t_{cycle} [s] is the total

400   cycle time, Q_{th} [J mol^{-1}] is specific heat, $t_{des,end}$ [s] is the time at the end of the desorption step,

401   $t_{heat,start}$ [s] is the time at the start of the heating step, W [J mol^{-1}] is specific work, $t_{vac,end}$ [s] is the

Email: jpy1@hw.ac.uk   RCCS, Heriot-Watt University

402   time at the end of the vacuum step, $t_{vac,start}$ [s] is the time at the start of the vacuum step, n_i [mol s^{-1}]

403   is the molar flow rate of component i, N_c [-] is the number of components, η_{vac} [-] is the isentropic

404   vacuum pump efficiency, γ_{gas} [-] is the heat capacity ratio of the gas, and η_{blower} [-] is the isentropic

405   blower efficiency. Purity is calculated, assuming that all the water can be condensed out in the

406   compression process.

407   The specific thermal energy is subsequently converted to specific equivalent work via the Carnot

408   efficiency as per the guidance of Danaci et al.[61] This allows for both forms of specific energy, thermal

409   and work, to be collected into one term. The equation for this conversion is shown in Equation 24.

$$W^{eq} = W + \eta_{turb}\left(1 - \frac{T_L}{T_H}\right)Q_{th} \qquad 24.$$

410   Here W^{eq} [J mol^{-1}] is the specific work equivalent, η_{turb} [-] is an isentropic turbine efficiency, T_L

411   [K] is the lowest temperature that energy can be extracted at, whilst T_H [K] is the temperature of the

412   heating medium in the system. T_L is assumed to equal to the ambient feed temperature, whilst T_H is

413   equal to T_j during the heating step. η_{turb} is taken as 0.75 since Danaci et al. state that values between

414   0.7 and 0.8 are appropriate.[61]

415   The physical packed-bed column model was implemented in the gPROMS custom modelling suite.[62]

416   The partial differential equations were first discretised using a 2nd order central finite differences

417   method. Next, the index of the equations is reduced according to the Pantelides algorithm to create a

418   solvable set of ordinary differential equations.[63] Finally, these ordinary differential equations were

419   solved using an implicit Runge-Kutta method and a variable time step. Cyclic steady-state conditions

420   are evaluated at 5 equidistant points along the column. Cyclic steady-state is defined as when the

421   loading, composition, pressure and temperature at each of these points at the end of the cycle is within

422   0.5% of the values at the end of the previous cycle. There is also the option in the model to monitor the

423   percentage of CO_2 saturation reached at the end of the bed during the cycles. This can be used to adjust

424   the adsorption time accordingly, as is done in this work's parametric study.

4.3 HEURISTIC PROCESS OPTIMISATION

426   Finally, a heuristic optimisation was performed in order to compare the performance indicators when

427   using the different co-adsorption isotherm models in the cycle model. The heuristic optimisation

428   approach involves varying many operating variables simultaneously to try and find the optimal design

429   space. To that end, we used gPROMS Global Systems Analysis tool, and more specifically the Monte

430   Carlo-based method function. The baseline case, described fully in Table S9 of the supplementary

431   information, is the starting point for this work and is also used to compare the cycle profiles using each

432   co-adsorption isotherm model. Monte Carlo simulations are done varying five main operating variables

433   in the process: vacuum pressure, jacket temperature, heating time, desorption time, and adsorption time.

Email: jpy1@hw.ac.uk   RCCS, Heriot-Watt University

434 Instead of controlling the adsorption time directly, the percentage of CO_2 saturation reached at the end

435 of the bed is controlled. For each variable, a uniform distribution was assumed between the low and

436 high values. These values are detailed in Table 1.

437 Sonnleitner et al. found that the stability limit of Lewatit VP OC 1065 ® is 90°C and 110°C in air

438 and N_2, respectively.[52] It is assumed that oxygen is the reason why the stability limit is much lower in

439 air. By the time the column reaches these temperatures in our baseline case, the column's gas

440 composition is made up of mostly CO_2 and H_2O, so 100°C is chosen as a maximum limit. This is also

441 the operating limit defined by the manufacturer.[23] The lower limit of vacuum pressure is chosen to be

442 0.1 bar, as pressures below this value are not typically achieved on an industrial scale. There is no

443 specific limit on the rest of the parameters, and they were chosen after a preliminary investigation into

444 the operating region of interest.

445 The actual distribution of the factors can be found in the supplementary information, which confirms

446 that they are uniform. The one exception to this being the vacuum pressure distribution of the

447 simulations using the Stampi-Bombelli et al. model. It was observed that the model struggled to

448 converge at less deep vacuum pressures. However, this is not important as, at these vacuum pressures,

449 the purities using this isotherm model are generally very low, hence the results would not be carried

450 forward for further study. For each isotherm model, 3000 samples are simulated using the cycle model

451 to get a thorough design space coverage.

452 *Table 1 Low and high values for the factors in the heuristic optimisation, where the CO_2 bed saturation parameter is a proxy*
453 *for adsorption time. This value will be 100% when breakthrough is complete, and investigating higher adsorption times will*
454 *be pointless. Equally, very low values of this parameter indicate that breakthrough has just begun. Guaranteeing this is*
455 *above 0% ensures exploring adsorption times that equate to full bed utilisation.*

Variable	Unit	Low value	High value
P_{vac}	*bar*	0.1	0.45
$T_{j,heat}$ / $T_{j,des}$	°C	90	100
t_{heat}	*s*	100	1500
t_{des}	*s*	18000	24000
CO_2 bed saturation ($z = L, t = t_{ads,end}$)	%	95	99

456

5 RESULTS AND DISCUSSION

5.1 PURE COMPONENT EQUILIBRIA

459 The measured experimental isotherms for pure CO_2 and H_2O adsorption are shown in the

460 supplementary information, Figures S6 and S10, respectively, with the desorption branches included.

Email: jpy1@hw.ac.uk   RCCS, Heriot-Watt University

Additionally, the isotherm model fits to the adsorption branches are shown in Figures S7, S8, S9, and S11, whilst the fitted parameters for CO_2 adsorption are shown in Tables 2 and 3. It was decided that taking hysteresis into account in process modelling would make the cycle model solution unnecessarily complex, and there are questions over how the experimental desorption branches, based only on pressure reduction, would extrapolate to a process where temperature is also being increased.

Table 2 Temperature-dependent Toth model parameters from isotherm fitting. Note that this is for our adjusted version of the Toth model, where the affinity equation no longer includes the reference temperature.[§]

Parameter	Value	Unit
T_0	298.15	K
$q_{\infty,0}$	4.86	$mol\ kg^{-1}$
χ	0.0000	-
b_0	2.85×10^{-21}	Pa^{-1}
$-\Delta H_0$	117,798	$J\ mol^{-1}$
τ_0	0.209	-
α	0.523	-

We shall not go into many details on the pure-component isotherms since they have been explored many times before.[7,8,11,12,15] However, the hysteresis observed for both CO_2 and H_2O isotherms is interesting and for CO_2 adsorption measurements this is an unexpected insight. Careful attention was applied to ensuring each point of both the adsorption and desorption branches had reached equilibrium, e.g., by increasing the tolerance to move to a next step (mass change per time) from 0.0015% min[-1] to 0.0007% min[-1]. Evidence of this can be seen in the mass change over time gravimetric graph in the supplementary information, Figure S1. Thus, the alternative explanation that equilibrium was not entirely reached before stepping to the next measurement point was tentatively rejected and we believe the hysteresis exhibited is a real phenomenon.

Such hysteresis in CO_2 adsorption on amine-functionalised sorbents has been observed before in a study by Zhou et al. in 2014.[64] The adsorbent that the authors studied was an amine functionalised SBA-15. We agree with these authors' suggestion that the hysteresis is potentially due to the strongly chemisorbed species formed on adsorption, and an explanation can be found in the fact that the endothermic direction of the reaction (desorption), has a greater activation energy than the exothermic direction. This also explains how the hysteresis becomes less significant as temperature increases as generally, the energy to overcome this barrier is more likely to exist in the system. Previously, a study by Yu and Chuang has shown that some carbamic acid, the species with the highest heat of adsorption in paired form, is only desorbed using temperature-programmed desorption, supporting the explanation

---

[§]Limits were imposed on parameters during the fitting process to ensure that the parameters kept their physical meaning. For example, χ is limited to being greater than or equal to 0 to ensure that the maximum capacity did not increase with increasing temperature and so avoided the isotherms crossing.

Email: jpy1@hw.ac.uk   RCCS, Heriot-Watt University

486 provided here.[27] Meanwhile, the hysteresis loop exhibited in the H_2O isotherms, is common behaviour

487 for multilayer adsorption as a result of metastability of the multilayer in the adsorption branch.[19]

488   The fitting of the water isotherms was slightly more complicated due to the unknown nature of the

489 relationship between E_1 and E_{2-9} and temperature. A linear relationship was observed between E_{2-9}

490 and temperature in the temperature range studied, much like the latent heat of condensation, E_{10} .

491 Meanwhile, E_1 appeared to have a concave downwards relationship with temperature meaning the

492 difference between the heat of adsorption of E_1 and E_{2-9} reduces as temperature increases. This is

493 shown in Figure S12 in the supplementary information. Equations 25 and 26 show the correlations that

494 will fit these two relationships.

$$E_1 = C - \exp(DT) \qquad\qquad 25.$$

$$E_{2-9} = F + GT \qquad\qquad 26.$$

495   Where $C, D, F,$ and G are constants. The fitted values of these constants can be found in Table 3.

496 *Table 3 Model parameters fitted to the temperature-dependent GAB model, including correlations in Equations 25 and 26.*

Parameter	Value	Unit
q_m	3.63	$mol\ kg^{-1}$
C	47110	$J\ mol^{-1}$
D	0.023744	K^{-1}
F	57706	$J\ mol^{-1}$
G	-47.814	$J\ mol^{-1}K^{-1}$

497   Additionally, the average isosteric heats of adsorption as calculated from the Clausius-Clapeyron

498 relation using the experimental isotherm data were -70 kJ mol^{-1} and -46 kJ mol^{-1} for CO_2 and H_2O

499 adsorption, respectively.

5.2 CO-ADSORPTION EQUILIBRIA

501   Figure 6 presents the CO_2 isotherm results under wet conditions. Here, we present the uptake

502 enhancement as a function of relative humidity and CO_2 pressure, where the enhancement factor is

503 defined as the CO_2 adsorption under wet conditions divided by the CO_2 adsorption under dry conditions

504 at the same temperature and partial pressure of CO_2. The co-adsorption enhancement effect primarily

505 manifests itself in the lower pressure region with up to 2.5 times the adsorption capacity as under dry

506 conditions. This is of key importance for DAC processes, as they operate adsorption at partial CO_2

507 pressures of 0.4 mbar. The enhancement seems to asymptote towards unity in the higher-pressure

508 region. Again, this is beneficial for DAC, as desorption commences at significantly higher partial

509 pressures than adsorption (e.g., ~ 30 mbar in the baseline case considered in Figure 12).

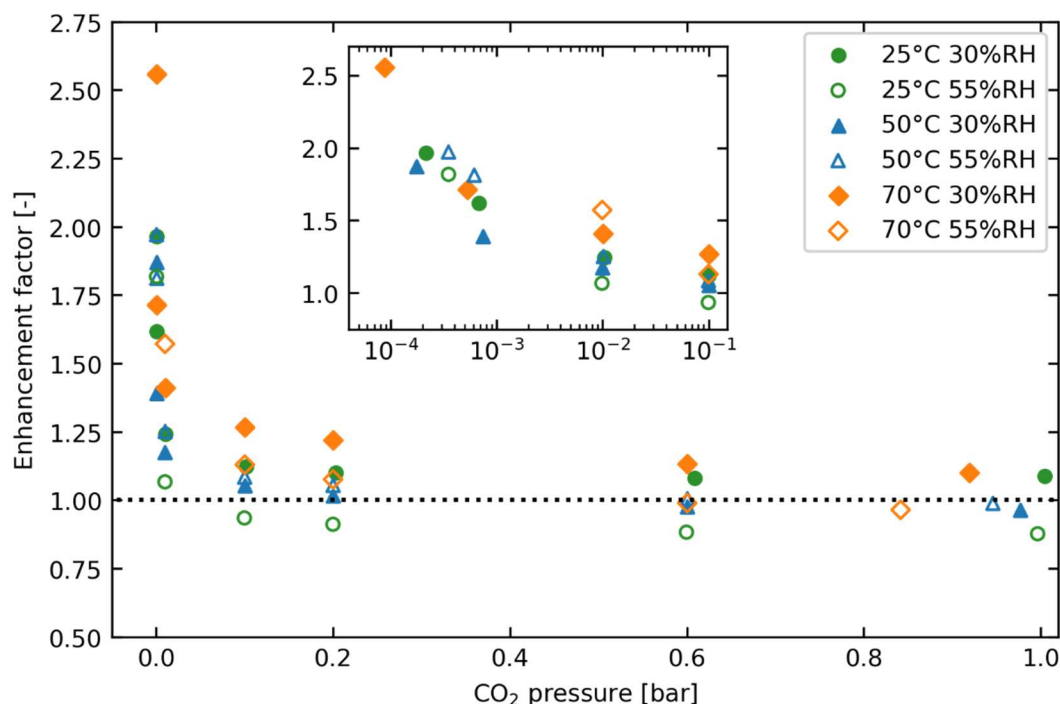Email: jpy1@hw.ac.uk   RCCS, Heriot-Watt University

Figure 6 Enhancement factor of co-adsorption experiments plotted against pressure for a range of temperatures and humidities. Here enhancement factor is defined as amount of CO_2 adsorbed divided by the amount of CO_2 that would be adsorbed under dry conditions at the same temperature and pressure. The isotherm loading values can be found in Figure 7. Meanwhile, they are converted into amine efficiency in Figure S13 in the supplementary information using the amine loading of $6.7 mmol\ g^{-1}$ reported by Alesi and Kitchin.[37]

The observation that the enhancement of CO_2 adsorption occurs mainly at lower CO_2 pressures supports the theory that carbamic acid formation is the main adsorption mechanism on Lewatit® VP OC 1065 as earlier suggested by molecular modelling from Buijs and De Flart.[36] (See Figures 1b and 2b in Section 2.2.1) If ammonium bicarbonate or hydronium carbamate was formed from ammonium carbamate, the high enhancement factors observed at low partial pressures would be expected to persist at higher partial pressures as each amine group that is used for adsorbing one CO_2 molecule under dry conditions can now adsorb two. (See Figures 1a and 2a in Section 2.2.1) Indeed, the ϕ_{dry} in the mechanistic model is fitted to have a value of 1, suggesting that under dry conditions the same stoichiometry exists as under wet conditions. In addition, Stampi-Bombelli et al. fitted their γ parameter to be 0 on amine-functionalised cellulose, meaning that the maximum adsorption capacity was not affected by water. This is further evidence against an increase in stoichiometry. For these reasons, we believe that paired carbamic acid and water-stabilised carbamic acid are the two main species formed due to CO_2 adsorption. However, this does not mean that ammonium carbamate cannot form, and this has been proven to happen on other adsorbents.[25,27,29–32] An alternative explanation is that ammonium carbamate forms under dry conditions, but the presence of water promotes carbamic acid formation instead, as suggested by Yu and Chuang.[27]

The co-adsorption results of Figure 6 also seem to indicate that the higher-humidity experiments sit slightly below the lower-humidity experiments, even reducing the enhancement to below 1 at higher

Email: jpy1@hw.ac.uk   RCCS, Heriot-Watt University

529 partial pressures, which seems apparent especially for the 25°C and 70°C measurements. This would
530 suggest that water can indeed block some amine sites and thereby lower adsorption capacity, as we
531 hypothesised in Section 2.3.1, but it is difficult to say for sure if this is true as this effect was not visible
532 in the 50°C experiment. The experiments were repeated to check this, with identical results obtained.
533 Therefore, further experimentation including different experimental methods needs to be undertaken:
534 currently, we are running a campaign of breakthrough experiments that could corroborate or reject the
535 findings here.

536
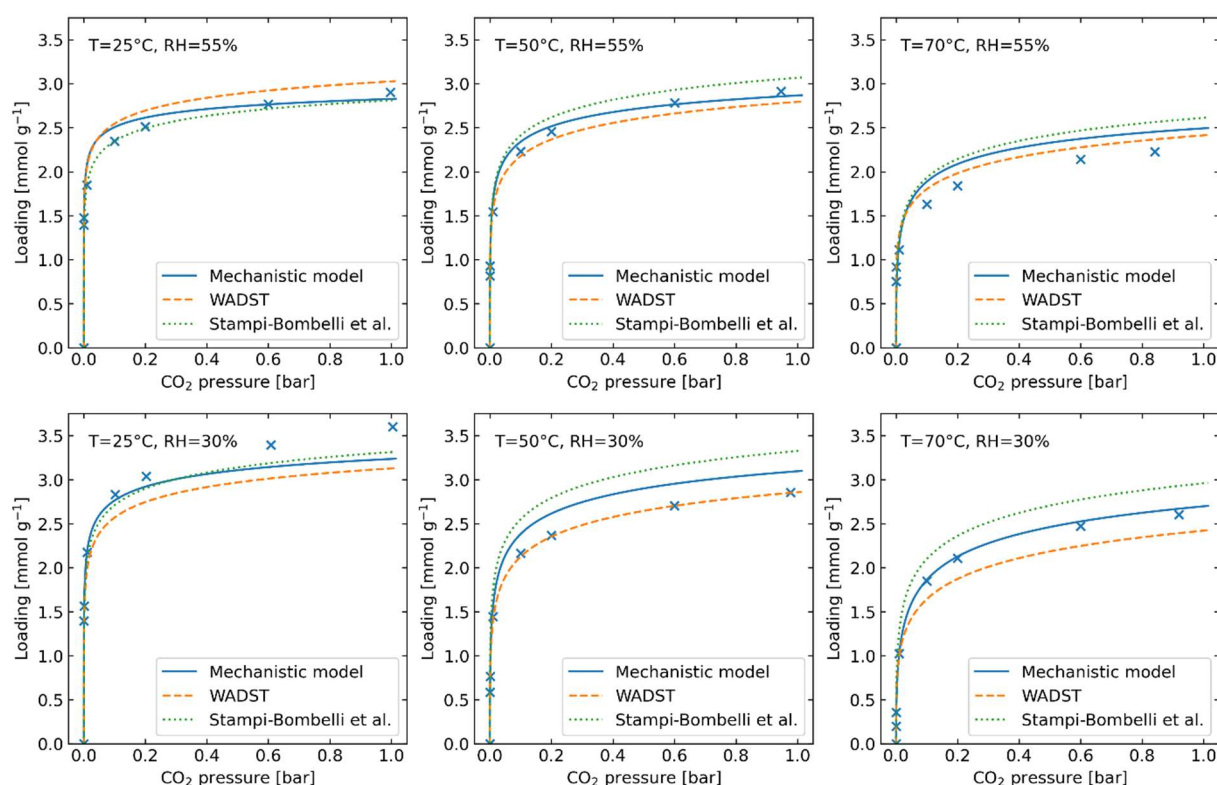
Figure 7 Experimental co-adsorption CO_2 isotherms (markers), at various temperatures (T) and relative humidities (RH), fitted to an empirical literature co-adsorption model from Stampi-Bombelli et al. and the two models presented in this work.[13] The low pressure range of this graph on a log scale is presented in Figure S14 in the supplementary information.

537

538 Figures 7 and S14 shows the fit of the experimental data to the two novel co-adsorption models in
539 this work alongside the empirical model from Stampi-Bombelli et al.[13] The parameters found in this
540 fitting process are presented in Table 4. It is noted that no model provides a perfect fit, and there is at
541 least one case for each model where a relatively poor fit is found, indicating the known and unknown
542 complexities of co-adsorption and measuring it. When comparing the three models, it is observed that
543 the WADST and the mechanistic model seems to fit the low-pressure region very well. The low-
544 pressure region is most important for DAC, as the partial pressure of CO_2 is always relatively low
545 throughout the cycle, hence this is especially promising. Furthermore, we suggest that there could be
546 changes in the mechanisms at higher CO_2 pressures and this explains why the fitting is generally poorer

Email: jpy1@hw.ac.uk   RCCS, Heriot-Watt University

at the higher-pressure regions. The mechanistic model seems to predict the higher-pressure region better than the WADST model, although the predictions are far from perfect.

Meanwhile, the Stampi-Bombelli et al. consistently overpredicts the capacity at the higher two temperatures. We suggest this is due to the model not considering the effect of temperature on the co-adsorption phenomenon. Mathematically, for a given water loading, it is predicting a constant increase in affinity and decrease in capacity at every temperature.

Another important point to make is that the experimental data has sources of potential error. We are trying to elucidate the effect of three parameters (temperature, pressure, and humidity) at once, and there is a possibility for measurement error in all these as well as in the sample mass. Considering this, we should not expect the models to be able to fit the experimental data perfectly.

Finally, when studying the fitted parameters, the value of the critical water loading parameter, A, is very similar in both the WADST model and the mechanistic model. This is noteworthy as it implies that both models predict the same probability of a CO_2 adsorption site having a water molecule available given the same loading of water, which is supportive of our hypotheses on co-adsorption.

Table 4 Fitted parameters for the empirical literature co-adsorption isotherm model and the two co-adsorption isotherm models presented in this work.

Parameter	Value	Unit
Stampi Bombelli et al. model		
γ	-0.137	-
β	5.612	-
Mechanistic model		
$f_{blocked,max}$	0.433	-
k	0.795	$kg\ mol^{-1}$
ϕ_{dry}	1.000	-
A	1.535	$mol\ kg^{-1}$
$-\Delta H_{wet}$	130155	$J\ mol^{-1}$
n	1.425	-
WADST model		
$b_{0,wet}$	1.230×10^{-18}	Pa^{-1}
$q_{\infty,0,wet}$	9.035	$mol\ kg^{-1}$
$\tau_{0,wet}$	0.053	-
χ_{wet}	0.000	-
α_{wet}	0.053	-
$-\Delta H_{wet}$	203687	$J\ mol^{-1}$
A	1.532	$mol\ kg^{-1}$

5.3 EFFECT OF CO-ADSORPTION MODEL SELECTION ON PROCESS MODELLING

5.3.1 Effect on working capacity for a fixed cycle

A key question we asked ourselves is if and how the selection of co-adsorption isotherm model influences performance predictions of DAC cycles. Figure 8 exemplifies how cycle profiles at the

Email: jpy1@hw.ac.uk   RCCS, Heriot-Watt University

567 column end ($Z = L$) may vary as different co-adsorption isotherm models are used for the baseline DAC
568 cycle specified in the supplementary information, Table S9. It is not a surprise that for most of the
569 monitored variables (q_{H_2O}, x, T, and P), there is no significant effect of including a co-adsorption
570 description, the exception being the CO_2 loading and mole fraction. Notably, the loading at the start and
571 the end of the desorption step varies significantly depending on the chosen description. These values
572 influence the working capacity of the material, which is the main difference when considering the cycle
573 profiles. This is important since the working capacity will have a substantial impact on process
574 performance since it is defined as the amount of CO_2 recovered in one cycle. The WADST and
575 mechanistic isotherm models lead to similar predictions of a greater working capacity than when no co-
576 adsorption is included, predicting ~50% higher loadings during the adsorption step and ~30% higher
577 loadings after desorption, effectively increasing cyclic working capacity by ~50%.

578 In contrast, the Stampi-Bombelli et al. approach leads to a similar working capacity to when no co-
579 adsorption is included. This is due to the model assuming that the effect of water loading on the isotherm
580 parameters varies with water loading but not temperature, meaning that this model also predicts higher
581 loadings at desorption conditions. Meanwhile, the WADST and mechanistic models do take the effect
582 of temperature on co-adsorption into account. This leads to the enhancement predicted by the WADST
583 and mechanistic models being higher at the start of the desorption step yet lower at the end than the
584 empirical model predicts.

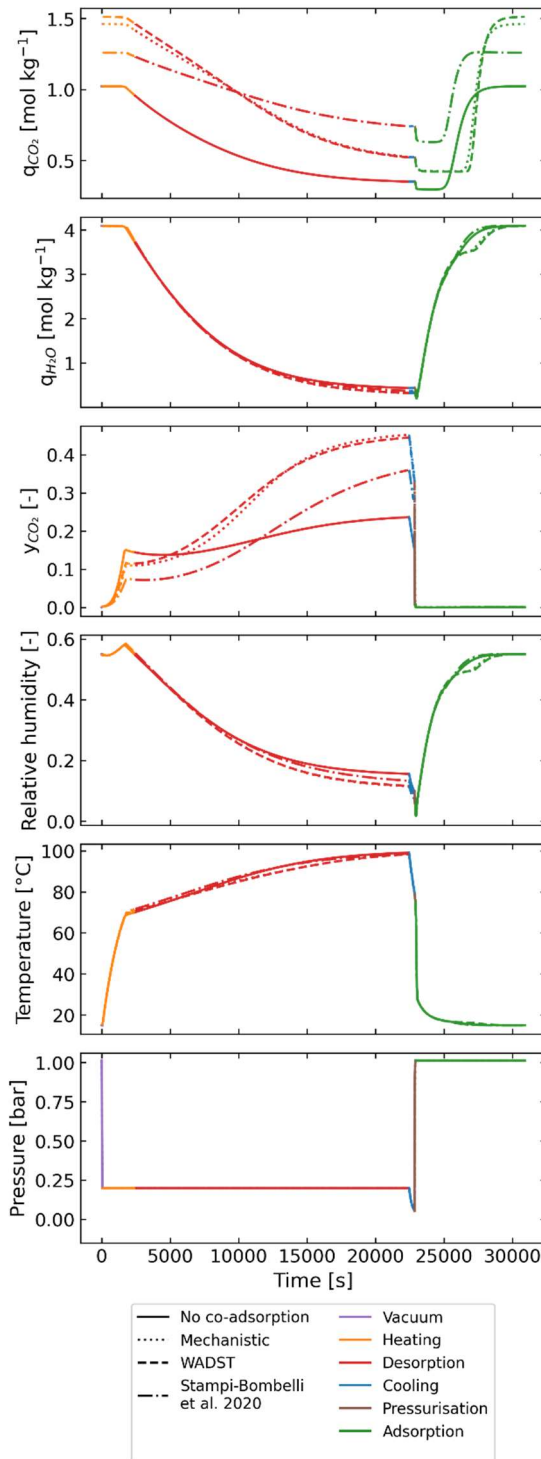Email: jpy1@hw.ac.uk   RCCS, Heriot-Watt University

Figure 8 Modelled cyclic steady-state profiles at the end of an adsorption column (Z = L) for the TVSA DAC baseline case using 4 different co-adsorption isotherm models. From top to bottom: CO_2 loading, H_2O loading, CO_2 mole fraction in the gas phase, relative humidity, temperature, and pressure.

585

5.3.2 Effect on purity, specific work equivalent, and productivity

587   The effects of co-adsorption and the specific model selection are further exemplified by the heuristic

588   optimisation results, exhibited in Figures 9. As previously discussed, the working capacity is the

26

primary variable being affected by the co-adsorption description. Hence, the difference in working capacities is a solid explanation of why the distributions vary significantly. However, there are other factors at play. The main one being the shape of the isotherm, which influences the pressure and temperature variation necessary to achieve a specific working capacity.
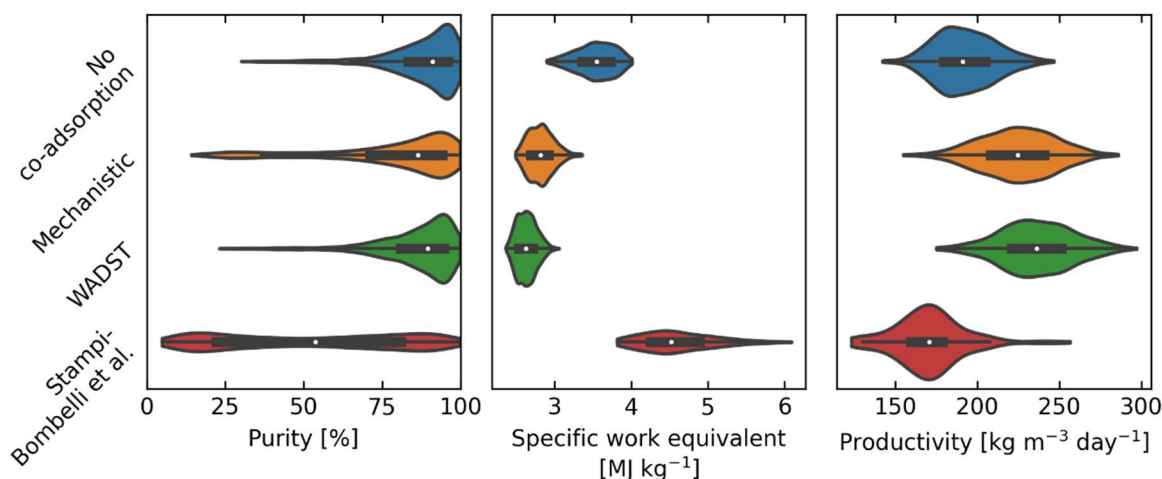
Figure 9 Violin plots of purity, specific work equivalent, and productivity produced by the parametric study of the TVSA DAC process, using the 4 different approaches to modelling co-adsorption. Specific work equivalent and productivity are shown after removing samples with purity less than 95%. The white dot is the median, the black bar is the interquartile range, the black line is the adjacent values, and the coloured area is the distribution represented by a kernel density estimator.

A good example materialises when comparing the mechanistic and WADST model points, selected as they have identical working capacities, in Table S11 of the supplementary information. The mechanistic model predicts that a lower vacuum pressure, longer heating time and longer desorption time are needed to achieve the same working capacities. This is caused by the slight difference in the shape of the isotherm and its dependency on temperature. Essentially, the mechanistic model predicts a higher affinity at higher temperatures. Overall, comparing the mechanistic model to the WADST model (considering the working capacities are identical):

- The lower vacuum pressure leads to a higher electrical energy requirement.
- The overall combined longer heating and desorption time leads to i) a lower productivity, and ii) a slightly higher heating requirement, as a slightly higher final temperature is achieved.

This reflects what we see in the distributions with the mechanistic model predicting slightly higher work equivalent and lower productivity. The slight difference in purity is again due to the isotherm shape and can be explained by considering that a longer heating time is required in the mechanistic model case, hence CO_2 starts desorbing at higher temperature. So, the lower purity values predicted are explained by the heating time simply being too short to desorb enough CO_2 to displace the N_2 from the column.

The same arguments can be made when analysing the no co-adsorption, and Stampi-Bombelli et al. cases. The Stampi-Bombelli et al. model predicts a very steep isotherm at low partial pressures of CO_2 and regeneration temperatures, leading to the requirement for much lower vacuum pressures to achieve comparable working capacities. So, the electrical work, hence work equivalent, is predicted to be much higher than for the other models, and at the same time, the distribution of purity is larger as only the data points with such low vacuum pressures deliver viable purities. The no co-adsorption case predicts the lowest working capacities at optimal conditions leading to distributions of lower productivities and higher specific work equivalent than for the mechanistic and WADST model cases. However, the isotherm is the least steep at low pressures. So, despite the low working capacities, the work equivalent distribution predicted is better than for the Stampi-Bombelli et al. case since less extreme vacuum pressures are required to achieve the desired purity. Likewise, this is why the no co-adsorption predicts the largest share of high purities of all the models.

To summarise, the mechanistic and WADST model predict that co-adsorption improves process performance, in terms of productivity and specific work equivalent, due to the higher achievable working capacities. However, it does make it slightly harder to achieve the required purity, as the isotherms have a larger gradient in the lower-pressure region. Meanwhile, the Stampi-Bombelli et al. isotherm model predicts that co-adsorption penalises process performance due to requiring deeper vacuum pressures owing to a higher affinity. It is expected that if a lower vacuum pressure limit was chosen, the Stampi-Bombelli et al. model case would achieve the desired purity more easily. This leads to a perhaps obvious but interesting conclusion that there is an optimal gradient in the lower-pressure region. It needs to be steep enough to adsorb CO_2 at such low concentrations, without being too steep, at desorption temperatures and partial pressures, to require very deep vacuum pressures. Meanwhile, this gradient is affected by both the affinity constant, b, of the sorbent in dry conditions, and the humidity.

Overall, the findings of the Stampi-Bombelli et al. model are cautiously rejected based on its failure to predict the capacity of the sorbent at higher temperatures, see Section 5.2. However, it does present itself as a valuable option if only the adsorption at one temperature is subject of study.

5.3.3 Optimal cycle designs and operating points.

Then, the question of how the co-adsorption models affect *optimal* cycle design and trends in process performance is answered by investigating Figure 10, and Figures S23-S26 in the supplementary information. Also in the supplementary information is Table S10, which shows the points from Figure 10, optimising one of the performance indicators. Figure 10 shows Pareto fronts of productivity and specific work equivalent predicted using each isotherm modelling approach.

Beginning with the common trends, a higher heating temperature always leads to better performance concerning specific work equivalent and productivity until it reaches the chosen degradation

temperature limit of ~100°C. Furthermore, cycle performance is improved when we run the adsorption step until the sorbent is practically completely saturated, allowing CO_2 to breakthrough at the column end (this is contrary to post-combustion capture, where it is vital to achieve high recoveries, as the main goal is to prevent CO_2 emissions to the atmosphere). Additionally, vacuum pressure and the heating time present a trade-off between productivity and specific work. Operating at a higher vacuum pressure leads to lower specific equivalent work, as a higher proportion of the desorption energy is supplied via heat which is less valuable in terms of exergy. However, then a longer heating time - reducing productivity - is needed to ensure that the most of the N_2 is displaced prior to desorption to achieve the desired purity.

Now, considering which co-adsorption models lead to the best DAC performance predictions, the WADST and mechanistic models clearly predict better performance as a result of co-adsorption (for the constraint of greater than 95% purity). The Pareto front is much shorter when these co-adsorption descriptions are applied, implying that there is a diminished trade-off between productivity and energy consumption, demonstrating that the operating conditions must be selected more cautiously to find the optimal point. One notable difference as discussed earlier, is the predicted optimal vacuum pressure which is lower when a co-adsorption description is included. It may be worth investigating whether even lower vacuum pressures can be achieved in actual equipment at an industrial scale. The minimum vacuum pressure was chosen as 0.1 bar since it was assumed that it might be significantly harder to achieve lower pressures: in industrial settings, vacuum pressures are usually higher than 0.1 bar.

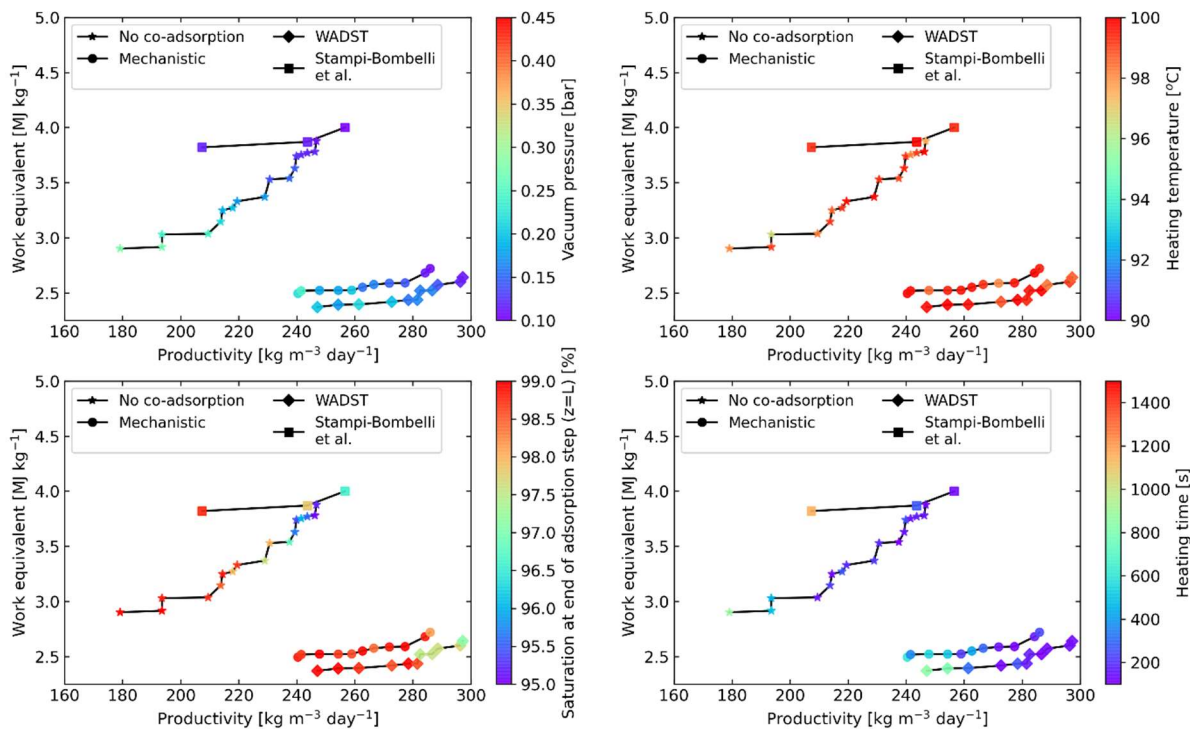Email: jpy1@hw.ac.uk   RCCS, Heriot-Watt University

Figure 10 Pareto fronts of specific work equivalent vs productivity for samples that show a purity of greater than 95% as predicted when applying each co-adsorption isotherm model approach. The operating parameter desorption time is left out as there is no obvious trend on the pareto front. Solid lines added as a guide for the eye. The range of the colour bars is the range investigated in the heuristic optimisation. We see here that the heating temperature converges to the upper bound for all values on the pareto front. A breakdown of the work equivalent contributions for the optimal points can be found in Figures S27 in the supplementary information.

5.3.4 Benchmark for a solid-sorbent DAC process

Finally, with the previously obtained results and insights, the energy consumption of an optimised DAC process using a commercially available sorbent could be benchmarked.[**] The mechanistic co-adsorption isotherm model is used as its mechanistic nature suggests the highest accuracy when extrapolating beyond measured state parameters. It is also shown to be highly accurate in the all-important lower-pressure regions of the isotherm and is the more conservative out of the two novel co-adsorption isotherm models presented in this work. Here, we shall benchmark the process using specific work equivalent as it represents a useful performance indicator that takes into account the relative values of heat and electricity for a very general case. However, there may be situations, for example, if heat is very cheap due to waste heat being available, when it is more desirable to minimise electrical energy consumption.

Table 5 A comparison of the benchmark, Lewatit® VP OC 1065 minimum work equivalent case, modelled using the mechanistic isotherm model, compared to other DAC technologies. Additionally, the electrical work required to compress CO_2

[**]The authors believe that the heuristic optimisation represents a realistic DAC case when a co-adsorption description is included. The only parameter which is still uncertain is the heat transfer coefficient, and experimental data from a scaled-up unit is required to estimate this accurately. In any case, the sensitivity analysis in Figure S28 of the supplementary information shows that the heat transfer coefficient does not have a large effect on the work equivalent or purity of the process. It does have a significant impact on productivity, however.

Email: jpy1@hw.ac.uk   RCCS, Heriot-Watt University

Process	Packed-bed temperature vacuum swing adsorption		Coated monolith temperature vacuum swing adsorption with steam stripping		Liquid absorption
Material	Lewatit® VP OC 1065	Unknown – Climeworks process	MIL-101(Cr)-PEI-800	mmen-Mg_2(dobpdc)	Metal hydroxide
Working capacity [mol kg^{-1}]	0.91	Unknown	0.75	2.55	N/A
Specific heat energy [MJ kg^{-1}]	9.93	11.9	9.68	4.75	5.84
Specific electrical energy [MJ kg^{-1}]	0.80	2.52	0.80	0.73	1.46
Regeneration temperature [°C]	100	~100	100	100	~900
Specific work equivalent [MJ kg^{-1}]	2.49	4.55	2.45	1.54	4.76
Specific work equivalent [MJ kg^{-1}] (with additional compression to 150 bar)	2.93	4.99	2.89	1.98	4.76
Reference	This work	[65]	[66,67]	[66,67]	[68]

681

682   Table 5 compares this benchmark case to other DAC technologies in literature. The technologies

683   chosen for comparison are: i) the Climeworks process using average recorded values recently

684   reported[65], ii) two cases of a monolithic adsorption process using novel metal-organic frameworks

685   (MOFs)[66,67], and iii) a liquid absorption process. The monolithic adsorption case is believed to be a

686   similar technology to that used by Global Thermostat, albeit they are unlikely to be using such a novel

687   adsorbent, meanwhile the liquid absorption case is similar to that used by Carbon Engineering.[69,70]

688   We believe that using Lewatit® VP OC 1065 in a packed-bed TVSA process represents a realistic

689   benchmark due to the commercial availability of the sorbent and the simple set-up of the process. The

690   calculated heat input into this benchmark is 17% lower than the value reported for Climeworks. This is

691   not unexpected as our case represents a highly ideal and optimised situation. For example, given the

692   Climeworks adsorption bed design (compare, e.g., US patent 2017/0326494 A1),[71] it is not expected

693   that they can fully saturate their bed, as our models predict is the optimal case. Also, their electrical

694   energy consumption is higher by 215%. Explanations for this may lie in the performance of blowers

695   and vacuum equipment having significantly lower efficiencies during real operations, and in bed

696   pressure drop being much higher than predicted by our model (note that our model assumes a thin layer

697   of sorbent where the air flows through in axial direction, while in the CW contactor, the flow is parallel

698   to the adsorbent sheets, then permeates through the sheet, after which it flows parallel along the sheet

699   to the outlet again. As a result, our benchmark specific work equivalent is lower than for the Climeworks

Email: jpy1@hw.ac.uk   RCCS, Heriot-Watt University

process, suggesting that the Climeworks design could be further optimised to use less electricity and to maximise adsorbent use.

The predicted heat and electrical energy consumption of the monolithic adsorption process utilising MIL-101(Cr)-PEI-800 is similar to that predicted by the benchmark case. However utilising mmen-Mg_2(dobpdc) in a monolithic adsorption process leads to substantially lower heat and electrical energy consumption. The same research group has since shown that mass transfer limitations and the shape of the isotherm could reduce the effectiveness of mmen-Mg_2(dobpdc) for DAC[72] although, if these limitations can be overcome, functionalised MOFs could become effective DAC sorbents.

Last, the liquid absorption process uses less heat than our adsorption benchmark. However, this process is penalised in the work equivalent calculation due to the very high-temperature requirement for regeneration (~900°C), and as a result, it is the least favourable process using this metric. However it has been noted previously that, currently, the capital costs of this process may be lower than for solid sorbent based DAC.[73]

6   CONCLUSIONS

We have developed two novel approaches to modelling the co-adsorption of water and CO_2 onto chemical adsorbents, the 'mechanistic' and 'WADST' models, and showed, using a detailed DAC model, how the choice of (co-)adsorption isotherm significantly influences DAC process performance, as well as presented an independent benchmark of a TVSA process for direct air capture. To this end, we presented a comprehensive set of new pure-component isotherm data for CO_2 and H_2O adsorption on Lewatit® VP OC 1065, as well as co-adsorption isotherm data that shows the enhancement, and potential diminution at higher partial pressures, of CO_2 adsorption in the presence of water. The pure-component experimental data was fitted to the Toth isotherm model for CO_2 adsorption and the GAB isotherm model for water adsorption, the novel mechanistic and WADST co-adsorption models were fitted to the co-adsorption data and a comparison was made with an empirical model presented earlier. The WADST and mechanistic models were especially successful at fitting the co-adsorption data in the crucial lower-pressure region.

It was found that the WADST and mechanistic isotherm models both provide relatively similar results. The DAC cycle performance that they predict is improved due to co-adsorption, where the mechanistic model predicts slightly lower productivity, and higher specific energy input than the WADST model. We presented a benchmark DAC process-sorbent combination using the mechanistic co-adsorption isotherm model, which was chosen due to its i) accuracy, ii) mechanistic nature, and iii) conservative predictions compared to the WADST model. Minimising the energy consumption, the specific work equivalent of the process was found to be 2.49 MJ kg^{-1}, achieving a CO_2 purity of 95.2%.

This compares to the Climeworks process's specific work equivalent of 4.55 MJ kg^{-1}, where the difference can likely be explained by the effects of bed saturation, heat losses and inefficiencies that move the real process away from the modelled scenario. Additionally, vital learnings on how to operate solid sorbent based DAC processes were elucidated from the Pareto fronts that resulted from heuristic optimisation. This demonstrated that it is optimal to use a heating temperature as high as this sorbent's stability allowed (100°C) and run the column until saturation has just been reached. The vacuum pressure, desorption time, and heating time should then be optimised according to the desired purity and desired placement along the Pareto front, i.e., either favouring higher productivity lowering capital costs, or lower energy consumption lowering operating costs.

In conclusion, this study critically showed the importance of including accurate co-adsorption descriptions in process modelling of solid sorbent DAC systems and the considerable effect co-adsorption has on process performance due to varying working capacity and isotherm shape. Further work needs to be done to properly characterise co-adsorption on amine-functionalised sorbents at higher relative humidities, which are commonly found in the real-world, and study the effect that co-adsorption has on mass transfer, subject of an ongoing investigation. Further to this, a full and independent techno-economic assessment should be performed on this benchmark sorbent-process system to properly benchmark the price of DAC today and to identify opportunities to drive the cost down in the future to support the scale-up of this vital technology.

7 AUTHOR CONTRIBUTIONS

Here are the details of the author contributions according to CRediT.

John Young contributed to the conceptualisation, formal analysis, investigation, methodology, software, validation, visualisation, and writing – original draft. Enrique García-Díez contributed to the investigation, methodology, and writing – review and editing. Susana Garcia contributed to the conceptualisation, formal analysis, funding acquisition, investigation, methodology, and writing – review and editing. Mijndert van der Spek contributed to the conceptualisation, formal analysis, funding acquisition, investigation, methodology, visualisation, and writing – review and editing.

8 CONFLICTS OF INTEREST

There are no conflicts to declare.

Email: jpy1@hw.ac.uk   RCCS, Heriot-Watt University

9 ACKNOWLEDGEMENTS

10 REFERENCES

1   V. Masson-Delmotte, P. Zhai, O. Pörtner, D. Roberts, J. Skea, P. R. Shukla, A. Pirani, C. Moufouma-Okia, C. Péan, R. Pidcock, S. Connors, J. B. R. Matthews, Y. Chen, X. Zhou, M. I. Gomis, E. Lonnoy, T. Maycokc, M. Tignor and T. Waterfield, *Global warming of 1.5°C. An IPCC Special Report on the impacts of global warming of 1.5°C above pre-industrial levels and related global greenhouse gas emission pathways, in the context of strengthening the global response to the threat of climate change,* 2018.

2   J. C. Minx, W. F. Lamb, M. W. Callaghan, S. Fuss, J. Hilaire, F. Creutzig, T. Amann, T. Beringer, W. de Oliveira Garcia, J. Hartmann, T. Khanna, D. Lenzi, G. Luderer, G. F. Nemet, J. Rogelj, P. Smith, J. L. Vicente Vicente, J. Wilcox and M. del Mar Zamora Dominguez, *Environ. Res. Lett.*, 2018, **13**, 063001.

3   S. Fuss, W. F. Lamb, M. W. Callaghan, J. Hilaire, F. Creutzig, T. Amann, T. Beringer, W. de Oliveira Garcia, J. Hartmann, T. Khanna, G. Luderer, G. F. Nemet, J. Rogelj, P. Smith, J. L. V. Vicente, J. Wilcox, M. del Mar Zamora Dominguez and J. C. Minx, *Environ. Res. Lett.*, 2018, **13**, 063002.

4   M. Fajardy and N. Mac Dowell, *Energy Environ. Sci.*, 2017, **10**, 1389–1426.

5   G. Realmonte, L. Drouet, A. Gambhir, J. Glynn, A. Hawkes, A. C. Köberle and M. Tavoni, *Nat. Commun.*, 2019, **10**, 3277.

6   N. Casas, J. Schell, R. Pini and M. Mazzotti, *Adsorption*, 2012, **18**, 143–161.

7   C. Gebald, J. A. Wurzbacher, A. Borgschulte, T. Zimmermann and A. Steinfeld, *Environ. Sci. Technol.*, 2014, **48**, 2497–2504.

8   R. Veneman, N. Frigka, W. Zhao, Z. Li, S. Kersten and W. Brilman, *Int. J. Greenh. Gas Control*, 2015, **41**, 268–275.

9   N. R. Stuckert and R. T. Yang, *Environ. Sci. Technol.*, 2011, **45**, 10257–10264.

10   Y. Kuwahara, D. Y. Kang, J. R. Copeland, P. Bollini, C. Sievers, T. Kamegawa, H. Yamashita and C. W. Jones, *Chem. - A Eur. J.*, 2012, **18**, 16649–16664.

11   R. Serna-Guerrero, Y. Belmabkhout and A. Sayari, *Chem. Eng. J.*, 2010, **161**, 173–181.

12   M. J. Bos, T. Kreuger, S. R. A. Kersten and D. W. F. Brilman, *Chem. Eng. J.*, 2019, **377**,

798   120374.

799   13   V. Stampi-Bombelli, M. van der Spek and M. Mazzotti, *Adsorption*, 2020, **26**, 1183–1197.

800   14   J. Toth, *Acta Chim. Acad. Sci. Hungaricae*, 1971, **69**, 311–317.

801   15   M. Hefti and M. Mazzotti, *Adsorption*, 2014, **20**, 359–371.

802   16   M. Hefti and M. Mazzotti, *Ind. Eng. Chem. Res.*, 2018, **57**, 15542–15555.

803   17   D. Marx, L. Joss, M. Hefti, R. Pini and M. Mazzotti, *Energy Procedia*, 2013, **37**, 107–114.

804   18   M. Hefti, L. Joss, D. Marx and M. Mazzotti, *Ind. Eng. Chem. Res.*, 2015, **54**, 12165–12176.

805   19   M. Thommes, K. Kaneko, A. V. Neimark, J. P. Olivier, F. Rodriguez-Reinoso, J. Rouquerol
806   and K. S. W. Sing, *Pure Appl. Chem.*, 2015, **87**, 1051–1069.

807   20   J. A. Wurzbacher, C. Gebald, S. Brunner and A. Steinfeld, *Chem. Eng. J.*, 2016, **283**, 1329–
808   1338.

809   21   R. B. Anderson, *J. Am. Chem. Soc.*, 1946, **68**, 686–691.

810   22   R. B. Anderson and W. Keith Hall, *J. Am. Chem. Soc.*, 1948, **70**, 1727–1734.

811   23   Lanxess, 2021.

812   24   P. J. Linstrom and W. G. Mallard, *J. Chem. Eng. Data*, 2001, **46**, 1059–1063.

813   25   S. A. Didas, M. A. Sakwa-Novak, G. S. Foo, C. Sievers and C. W. Jones, *J. Phys. Chem. Lett.*,
814   2014, **5**, 4194–4200.

815   26   Y. Kuwahara, D. Y. Kang, J. R. Copeland, N. A. Brunelli, S. A. Didas, P. Bollini, C. Sievers,
816   T. Kamegawa, H. Yamashita and C. W. Jones, *J. Am. Chem. Soc.*, 2012, **134**, 10757–10760.

817   27   J. Yu and S. S. C. Chuang, *Energy and Fuels*, 2016, **30**, 7579–7587.

818   28   W. Jung and K. S. Lee, *J. Nat. Gas Sci. Eng.*, 2020, **84**, 103489.

819   29   U. Tumuluri, M. Isenberg, C. S. Tan and S. S. C. Chuang, *Langmuir*, 2014, **30**, 7405–7413.

820   30   W. C. Wilfong, C. S. Srikanth and S. S. C. Chuang, *ACS Appl. Mater. Interfaces*, 2014, **6**,
821   13617–13626.

822   31   C. S. Srikanth and S. S. C. Chuang, *J. Phys. Chem. C*, 2013, **117**, 9196–9205.

823   32   X. Wang, V. Schwartz, J. C. Clark, X. Ma, S. H. Overbury, X. Xu and C. Song, *J. Phys. Chem.
824   C*, 2009, **113**, 7260–7268.

825   33   A. Danon, P. C. Stair and E. Weitz, *J. Phys. Chem. C*, 2011, **115**, 11540–11549.

826   34   Z. Bacsik, N. Ahlsten, A. Ziadi, G. Zhao, A. E. Garcia-Bennett, B. Martín-Matute and N.
827   Hedin, *Langmuir*, 2011, **27**, 11118–11128.

828   35   P. Jäger, C. N. Rentzea and H. Kieczka, in *Ullmann's Encyclopedia of Industrial Chemistry*,
829   Wiley-VCH Verlag GmbH & Co. KGaA, 2000, pp. 553–560.

830   36   W. Buijs and S. De Flart, *Ind. Eng. Chem. Res.*, 2017, **56**, 12297–12304.

831   37   W. R. Alesi and J. R. Kitchin, *Ind. Eng. Chem. Res.*, 2012, **51**, 6907–6915.

832   38   K. Li, J. D. Kress and D. S. Mebane, *J. Phys. Chem. C*, 2016, **120**, 23683–23691.

833   39   L. A. Darunte, A. D. Oetomo, K. S. Walton, D. S. Sholl and C. W. Jones, *ACS Sustain. Chem.
834   Eng.*, 2016, **4**, 5761–5768.

Email: jpy1@hw.ac.uk   RCCS, Heriot-Watt University

835   40   W. Chaikittisilp, J. D. Lunn, D. F. Shantz and C. W. Jones, *Chem. - A Eur. J.*, 2011, **17**,
836   10556–10561.

837   41   M. A. Sakwa-Novak and C. W. Jones, *ACS Appl. Mater. Interfaces*, 2014, **6**, 9245–9255.

838   42   S. A. Didas, A. R. Kulkarni, D. S. Sholl and C. W. Jones, *ChemSusChem*, 2012, **5**, 2058–2064.

839   43   S. A. Didas, R. Zhu, N. A. Brunelli, D. S. Sholl and C. W. Jones, *J. Phys. Chem. C*, 2014, **118**,
840   12302–12311.

841   44   A. Kolmogorov, *Izv. Akad. Nauk USSR Ser. Math.*, 1937, **1**, 355–359.

842   45   C. W. Price, *Acta Metall. Mater.*, 1990, **38**, 727–738.

843   46   M. Avrami, *J. Chem. Phys.*, 1939, **7**, 1103–1112.

844   47   M. Avrami, *J. Chem. Phys.*, 1940, **8**, 212–224.

845   48   M. Avrami, *J. Chem. Phys.*, 1941, **9**, 177–184.

846   49   J. . Maxwell, *London, Edinburgh, Dublin Philos. Mag. J. Sci. 4th Ser.*, 1860, **19**, 19–32.

847   50   J. . Maxwell, *London, Edinburgh, Dublin Philos. Mag. J. Sci. 4th Ser.*, 1860, **20**, 21–37.

848   51   J. W. Park, C. U. Kim and W. Isard, *Phys. A Stat. Mech. its Appl.*, 2012, **391**, 4883–4890.

849   52   E. Sonnleitner, G. Schöny and H. Hofbauer, *Biomass Convers. Biorefinery*, 2018, **8**, 379–395.

850   53   J. P. Young, V. Martis, S. Garcia and M. van der Spek, *11th Trondheim Conf. CO2 Capture,*
851   *Transp. Storage.*, in press

852   54   Surface Measurement Systems, 2021.

853   55   P. Bollini, S. Choi, J. H. Drese and C. W. Jones, *Energy & Fuels*, 2011, **25**, 2416–2425.

854   56   G. Calleja, R. Sanz, A. Arencibia and E. S. Sanz-Pérez, *Top. Catal.*, 2011, **54**, 135–145.

855   57   US 2020/0001224 A9, 2020.

856   58   L. Joss, M. Gazzani, M. Hefti, D. Marx and M. Mazzotti, *Ind. Eng. Chem. Res.*, 2015, **54**,
857   3027–3038.

858   59   E. Glueckauf, *Trans. Faraday Soc.*, 1955, **51**, 1540–1551.

859   60   S. Ergun, *Chem. Eng. Prog.*, 1952, **48**, 89–94.

860   61   D. Danaci, P. A. Webley and C. Petit, *Front. Chem. Eng.*, 2021, **2**, 1–11.

861   62   Process Systems Enterprise, gPROMS, www.psenterprise.com/products/gproms, 1997-2021

862   63   C. C. Pantelides, *SIAM J. Sci. Stat. Comput.*, 1988, **9**, 213–231.

863   64   L. Zhou, J. Fan, G. Cui, X. Shang, Q. Tang, J. Wang and M. Fan, *Green Chem.*, 2014, **16**,
864   4009–4016.

865   65   S. Deutz and A. Bardow, *Nat. Energy*, 2021, **6**, 203–213.

866   66   A. Sinha, L. A. Darunte, C. W. Jones, M. J. Realff and Y. Kawajiri, *Ind. Eng. Chem. Res.*,
867   2017, **56**, 750–764.

868   67   A. Sinha, L. A. Darunte, C. W. Jones, M. J. Realff and Y. Kawajiri, *Ind. Eng. Chem. Res.*,
869   2020, **59**, 503–505.

870   68   N. McQueen, M. J. Desmond, R. H. Socolow, P. Psarras and J. Wilcox, *Front. Clim.*, 2021, **2**,
871   38.

Email: jpy1@hw.ac.uk   RCCS, Heriot-Watt University

872   69   E. Ping, M. Sakwa-Novak and P. Eisenberger, *Int. Conf. Negat. CO2 Emiss. May 22-24, 2018,*
873   *Göteborg, Sweden*, 2018, 1–9.

874   70   D. W. Keith, G. Holmes, D. St. Angelo and K. Heidel, *Joule*, 2018, **2**, 1573–1594.

875   71   US 2017/0326494 A1, 2017.

876   72   L. A. Darunte, T. Sen, C. Bhawanani, K. S. Walton, D. S. Sholl, M. J. Realff and C. W. Jones,
877   *Ind. Eng. Chem. Res.*, 2019, **58**, 366–377.

878   73   R. Hanna, A. Abdulla, Y. Xu and D. G. Victor, *Nat. Commun.*, 2021, **12**, 368.

879

Email: jpy1@hw.ac.uk   RCCS, Heriot-Watt University